Scheduling HVAC Loads to Promote Renewable Generation Integration with Learning-based Joint Chance-constrained Approach

Ge Chen, *Member*, *IEEE*, Hongcai Zhang, *Senior Member*, *IEEE*, *Member*, *CSEE*, Hongxun Hui, *Senior Member*, *IEEE*, *Member*, *CSEE*, and Yonghua Song, *Fellow*, *IEEE*, *Fellow*, *CSEE*

***Abstract*—Integration of distributed renewable generation (DRG) in distribution networks can be effectively promoted by scheduling flexible resources such as heating, ventilation, and air conditioning (HVAC) loads. However, finding the optimal scheduling for them is not trivial because DRG outputs are highly uncertain. To address this issue, this paper proposes a learning-based joint chance-constrained approach to coordinate HVAC loads with DRG. Unlike cutting-edge works adopting individual chance constraints to manage uncertainties, this paper controls the violation probability of all critical constraints with joint chance constraints (JCCs). This joint manner can explicitly guarantee operational security of the entire system based on operators' preferences. To overcome intractability of JCCs, we first prove that JCCs can be safely approximated by robust constraints with proper uncertainty sets. A famous machine learning algorithm, one-class support vector clustering, is then introduced to construct a small enough polyhedron uncertainty set for these robust constraints. A linear robust counterpart is further developed based on the strong duality to ensure computational efficiency. Numerical results based on various distributed uncertainties confirm the advantages of the proposed model in optimality and feasibility.**

***Index Terms*—Demand-side flexibility, HVAC systems, joint chance constraints, renewable energies, support vector clustering.**

NOMENCLATURE

A. Indices

i	Index of buses.
m	Index of constraints.
n	Index of samples.
t	Index of hours.

B. Parameters

C_i	Heat capacity of building i (MWh/°C).
$d_{i,t}$	Heat load from indoor sources in the buildings connected to bus i in hour t (MW).
COP_i	Coefficient of performance of the HVAC system in building i (MW/MW).
$\overline{G}_{i,t}$	Nominal active power output of distributed renewable generator on bus i in hour t (MW).
g_i	Heat transfer coefficient between indoor and outdoor environments in building i (MW/°C).
$p^{\text{e}}_{i,t}$, $q^{\text{e}}_{i,t}$	Active and reactive base loads on bus i in hour t (MW).
$\overline{p}_i$	Upper bound of the HVAC's active power in building i (MW).
r_{ij}, x_{ij}	Resistance and reactance of branch (i,j) (p.u.).
$S^{\max}_{ij}$	Maximum allowable apparent power flow on branch (i,j) (MW).
$\boldsymbol{\alpha}$, $\boldsymbol{\beta}$	Dual variables in problem P-SVC. Note that they are fixed when solving P2.
ϵ	Risk parameter.
η^{buy}_t, η^{sell}_t	Unit price for purchasing and selling electricity ($/MWh).
$\overline{\theta}_i$, $\underline{\theta}_i$	Upper and lower bounds of the thermal comfort region in building i (°C).
θ^{out}_t	Outdoor temperature at hour t (°C).
ϕ_i	Power factor of the HVAC system in the buildings connected to bus i.

C. Uncertainties

$\xi_{i,t}$	The uncertain level of the active power output of the distributed renewable generator on bus i in hour t.
$\mathcal{U}_t$	Uncertainty set.

D. Variables

EC_t	Total cost in hour t ($).
G_t	Net active power at the substation in hour t (MW).
$\boldsymbol{o}$	Center of the minima sphere.
$p_{i,t}$, $q_{i,t}$	Active and reactive power injection on bus i in hour t (MW).
$p^{\text{HV}}_{i,t}$, $q^{\text{HV}}_{i,t}$	Active and reactive power of the HVAC system in building i in hour t (MW).
$P_{ij,t}$, $Q_{ij,t}$	Active and reactive power flows on branch (i,j) in hour t (MW).
$P^{\text{aux}}_{ij,t}$, $Q^{\text{aux}}_{ij,t}$	Auxiliary variables for extracting the quadratic constraint from chance constraints.
R	Radius of the minima sphere.

Manuscript received October 2, 2022; revised November 20, 2022; accepted December 29, 2022. Date of online publication March 3, 2023; date of current version February 25, 2025. This work is funded in part by the Science and Technology Development Fund, Macau SAR, China (File no. 0094/2024/AGJ and File no. 001/2024/SKL).

G. Chen, H. Zhang (corresponding author, email: hczhang@um.edu.mo), H. Hui and Y. Song are with the State Key Laboratory of Internet of Things for Smart City and Department of Electrical and Computer Engineering, University of Macau, Macao 999078, China.

DOI: 10.17775/CSEEJPES.2022.06580

$U_{i,t}$ Voltage of bus i in hour t (p.u.).
$\boldsymbol{y}_t$ Generic decision variable.
$\theta_{i,t}^{\text{in}}$ Indoor temperature of building i in hour t (°C).
ω_n Slack variable used in the support vector clustering.

I. Introduction

THE increasing penetration of renewable generation mitigates the demand for fossil energy. However, it also exacerbates the imbalance between demands and generation due to the stochastic characteristics of renewable generation [1]. As a result, much distributed renewable generation (DRG) has to be curtailed to maintain operational security. Fortunately, integration of DRG can be promoted by properly scheduling flexible sources in distribution networks [2]. Due to the natural ability of buildings to store heating/cooling power, heating, ventilation, and air conditioning (HVAC) loads can be regarded as desirable demand-side flexible sources [3], [4]. Hence, tons of scheduling methods have been proposed to realize proper coordination between HVAC loads and DRG. For instance, reference [5] proposed an aggregation method to identify operational flexibility of multiple buildings. Reference [6] developed a simplification method to model flexibility of large-scale HVAC systems. Reference [7] regarded HVAC loads as virtual battery systems and provided a control scheme to unlock their flexibility.

However, it is hard to predict DRG outputs perfectly due to their stochastic characteristics. Thus, uncertainties from forecasting errors of DRG must be considered during power scheduling to avoid constraint violations [8]. Robust optimization has traditionally been used to manage these uncertainties [9]. However, it is usually overly conservative because every constraint should be satisfied with all possible realizations of uncertainties. Chance-constrained programming (CCP) is an alternative method to manage uncertainties from DG in OPF [10]. It allows constraint violations with a small probability, so operators can effectively balance robustness and optimality based on their preferences. Reference [11] proposed a CCP-based framework to coordinate thermostatically controlled loads with uncertain DRG. Reference [12] leveraged CCP to handle uncertainties from DRG during the planning of integrated energy systems. Reference [13] developed a multi-period CCP framework to aggregate HVAC loads for reserve services. Reference [14] utilized a distributionally robust CCP method to schedule flexible loads and energy storage systems in distribution networks. Reference [15] proposed a fast distributionally robust CCP framework to utilize the load flexibility of HVAC loads for cost minimization. However, most CCP-based methods, including [12]–[15], control the violation probability of critical constraints individually. For a distribution system, violations of any constraint may affect operational safety. Therefore, system security is hard to guarantee for this individual manner because it does not restrict all critical constraints to be satisfied simultaneously with a predetermined probability [16]. For example, suppose a system has two security constraints, i.e., $a_1 \in \mathcal{A}_1$ and $a_2 \in \mathcal{A}_2$. Now we wish to maintain its system security with a probability of $1-\epsilon$, i.e., $\mathbb{P}((a_1 \notin \mathcal{A}_1) \vee (a_2 \notin \mathcal{A}_2)) \leq \epsilon$. If we individually describe the probability satisfaction of the two security constraints, i.e., $\mathbb{P}(a_1 \notin \mathcal{A}_1) \leq \epsilon$ and $\mathbb{P}(a_2 \notin \mathcal{A}_2) \leq \epsilon$, then the corresponding violation probability is $\mathbb{P}((a_1 \notin \mathcal{A}_1) \vee (a_2 \notin \mathcal{A}_2)) = \mathbb{P}(a_1 \notin \mathcal{A}_1) + \mathbb{P}(a_2 \notin \mathcal{A}_2) - \mathbb{P}((a_1 \notin \mathcal{A}_1) \wedge (a_2 \notin \mathcal{A}_2)) \leq 2\epsilon - \mathbb{P}((a_1 \notin \mathcal{A}_1) \wedge (a_2 \notin \mathcal{A}_2))$. Since the term $2\epsilon - \mathbb{P}((a_1 \notin \mathcal{A}_1) \wedge (a_2 \notin \mathcal{A}_2)) \geq 2\epsilon - \mathbb{P}(a_1 \notin \mathcal{A}_1) \geq \epsilon$, this individual manner may not be able to ensure system security with the pre-determined probability (i.e. $1-\epsilon$).

The violation probabilities of critical constraints should be jointly considered due to the security concern of power systems [17], [18]. Therefore, joint chance constraints (JCCs), which jointly describe these probabilities, are preferable for coordinating HVAC systems with DRG in distribution networks. Unfortunately, JCCs are much more intractable than individual ones [19]. Hence, much effort has been made to overcome this. Generally speaking, the published methods for handling JCCs can be divided into three categories.

1) Bonferroni Approximation

The Bonferroni approximation leverages multiple individual chance constraints (ICCs) to approximate an intractable JCC. For instance, reference [20] employed the Bonferroni approximation to handle JCCs in operating drinking water networks. References [21], [22] provided tighter upper bounds for the Bonferroni approximation to improve its optimality. However, it requires that the summation of all individual violation probabilities is no larger than the joint one to guarantee the feasibility of solutions [10]. Hence, some individual violation probabilities may be very small. In this case, the Bonferroni approximation may derive overly conservative solutions [17].

2) Scenario Approach

The scenario approach approximates JCCs by requiring constraints to be robust for a finite number of scenarios. With a sufficient number of scenarios, feasibility of the original JCC can be guaranteed [10]. Reference [23] utilized the scenario approach to approximate JCCs with scenario-wise deterministic scenarios. References [24], [25] designed box uncertainty sets to cover all scenarios and proposed a robust optimization-based inner approximation to reduce computational burdens. Other types of uncertainty sets, e.g., ellipsoids [26] or convex hulls [27], have also been combined with the scenario approach to improve optimality. However, the approach may still be overly conservative once some extreme samples of uncertainties are chosen as scenarios.

3) Sample Average Approximation

The sample average approximation (SAA) utilizes enough empirical samples to approximate the underlying true distribution of uncertainties. SAA introduces auxiliary binary variables to identify safe samples (satisfying all constraints) and unsafe samples (causing constraint violations). By restricting the total number of unsafe samples, JCCs can be approximated by sample-wise deterministic constraints. Note that SAA differs from the scenario approach by accepting small constraint violations. Hence SAA can potentially achieve better optimality [10]. SAA has been utilized to handle JCCs in power grid planning [28] and unit commitment [29]. However, since SAA needs to introduce many binary variables, it is computationally expensive.

This paper aims to design an energy- and time-efficient scheduling method to overcome the challenges above, i.e., overly conservative results or huge computational burdens. To achieve this goal, a novel scheduling approach is proposed. Its main contributions are threefold:

1) We propose a joint chance-constrained model to manage the uncertainties from DRG during the coordination of HVAC loads and DRG in distribution networks. The violation probabilities of all critical constraints are jointly considered, so that system security can be explicitly guaranteed with a high probability.

2) We design a robust approximation with a novel learning-based uncertainty set to replace intractable JCCs. By leveraging the one-class support vector clustering (OC-SVC) algorithm, we establish a small polyhedron uncertainty set to tightly cover most historical samples for an energy-efficient solution. We further prove that this uncertainty set can guarantee the feasibility of solutions. To the best of our knowledge, this is the first adoption of the OC-SVC-based uncertainty set for joint chance-constrained scheduling problems.

3) We develop a tractable robust counterpart for the OC-SVC-based uncertainty set. This counterpart is linear and can be easily solved by off-the-shelf solvers with guaranteed computational efficiency.

The rest of this paper is organized as follows. Section II provides the system model. Section III presents the procedure of the proposed model. Section IV discusses simulation results, and Section V presents the conclusion.

II. Problem Formulation

HVAC systems and DRG are usually connected to distribution networks. By properly designing the power schedule of HVAC systems, integration of uncertain DRG can be promoted to reduce the total cost of distribution networks. Indoor thermal discomfort should be avoided to guarantee the service quality of HVAC systems. The scheduling strategy should satisfy bus voltage and branch power flow limitations to ensure the system's operational security.

A. Modeling of Building Thermal Dynamics

Indoor temperature variation in buildings can be described by a widely-used energy conservation model,

$$\theta_{i,t}^{\mathrm{in}} = a_i^{\mathrm{in}}\theta_{i,t-1}^{\mathrm{in}} + a_i^{\mathrm{out}}\theta_{t-1}^{\mathrm{out}} + a_i^{\mathrm{h}}d_{i,t-1} + a_i^{\mathrm{q}}p_{i,t-1}^{\mathrm{HV}},\ \forall i \in \mathcal{I},\ \forall t \in \mathcal{T} \tag{1}$$

where $\theta_{i,t}$ and $\theta_{t-1}^{\mathrm{out}}$ are respective temperatures of the indoor and outdoor environments; $d_{i,t}$ is the heat load contributed by indoor sources (e.g., humans and electric devices); $p_{i,t}^{\mathrm{HV}}$ is the active power of the HVAC system; and

$$\begin{cases} a_i^{\mathrm{in}} = e^{-\frac{g_i\Delta t}{C_i}},\ a_i^{\mathrm{out}} = 1 - a_i^{\mathrm{in}}, \\ a_i^{\mathrm{h}} = \frac{1}{g_i}a_i^{\mathrm{out}},\ a_i^{\mathrm{q}} = -\mathrm{COP}_i a_i^{\mathrm{h}}, \end{cases} \quad \forall i \in \mathcal{I} \tag{2}$$

where C_i is the heat capacity of the building connected to the i-th node, g_i is the corresponding heat transfer coefficient between indoor and outdoor environments, and Δt is the length of the optimization time interval; COP_i is the coefficient of performance of the HVAC system. The reactive power of the HVAC system calculated by

$$q_{i,t}^{\mathrm{HV}} = \sqrt{(1-\phi_i^2)}/\phi_i \cdot p_{i,t}^{\mathrm{HV}},\ \forall i \in \mathcal{I},\ \forall t \in \mathcal{T} \tag{3}$$

where ϕ_i is the power factor of the i-th HVAC system. Due to thermal comfort requirements and device limitations, the indoor temperature and active power of HVAC systems are bounded by

$$\underline{\boldsymbol{\theta}} \le \boldsymbol{\theta}_t^{\mathrm{in}} \le \overline{\boldsymbol{\theta}},\ \boldsymbol{p}_t^{\mathrm{HV}} \le \overline{\boldsymbol{p}},\ \forall t \in \mathcal{T} \tag{4}$$

where $\underline{\boldsymbol{\theta}}$ and $\overline{\boldsymbol{\theta}}$ are the lower and upper bounds, respectively, of the comfortable range; $\overline{\boldsymbol{p}}$ is the upper limitation of the active power of HVAC systems.

B. Modeling of Distribution Networks

1) Operation Cost

The energy cost of a distribution network is the cost of purchasing electricity (the net power at the substation is positive) plus the profit from selling power to the upper-level grid (net power is negative),

$$EC_t = (\eta^{\mathrm{buy}}G_t^{\mathrm{buy}} - \eta^{\mathrm{sell}}G_t^{\mathrm{sell}})\Delta t,\ \forall t \in \mathcal{T} \tag{5}$$

$$G_t^{\mathrm{buy}} - G_t^{\mathrm{sell}} = G_t^{\mathrm{g}},\ G_t^{\mathrm{buy}} \ge 0,\ G_t^{\mathrm{sell}} \ge 0,\ \forall t \in \mathcal{T} \tag{6}$$

where EC_t is the energy cost at time $t \in \mathcal{T}$; η^{buy} and η^{sell} are the per-unit prices of electricity purchasing and selling, respectively, G_t^{buy} and G_t^{sell} are two auxiliary variables; G_t^{g} is the net power at the substation; Δt is the length of a time slot.

2) Nodal Power Injections

The nodal power injections can be expressed as[1]:

$$\boldsymbol{p}_t = -\boldsymbol{p}_t^{\mathrm{HV}} - \boldsymbol{p}_t^{\mathrm{e}} + \boldsymbol{G}_t^{\mathrm{DG}} * \boldsymbol{\lambda}_t,\ 0 \le \boldsymbol{\lambda}_t \le 1,\ \forall t \in \mathcal{T} \tag{7}$$

$$\boldsymbol{q}_t = -\boldsymbol{q}_t^{\mathrm{HV}} - \boldsymbol{q}_t^{\mathrm{e}},\ \forall t \in \mathcal{T} \tag{8}$$

where $\boldsymbol{p}_t^{\mathrm{HV}}$ and $\boldsymbol{q}_t^{\mathrm{HV}}$ are vector forms of $p_{i,t}^{\mathrm{HV}}$ and $q_{i,t}^{\mathrm{HV}}$, respectively; $\boldsymbol{G}_t^{\mathrm{DG}}$ and $\boldsymbol{\lambda}_t$ are the available output and utilization rate of DRG, respectively; $\boldsymbol{p}_t^{\mathrm{e}}$ and $\boldsymbol{q}_t^{\mathrm{e}}$ are the active and reactive base loads, respectively (i.e., the loads apart from the power demands of HVAC systems); "$*$" denotes element-wise multiplication. In practice, the available output of DRG is usually uncertain, which can be expressed as:

$$\boldsymbol{G}_t^{\mathrm{DG}} = \overline{\boldsymbol{G}}_t^{\mathrm{DG}} * (1 + \boldsymbol{\xi}_t),\ \forall t \in \mathcal{T} \tag{9}$$

where $\overline{\boldsymbol{G}}_t^{\mathrm{DG}}$ and $\boldsymbol{\xi}_t$ are the nominal available power and uncertain level of DRG, respectively.

3) Power Flow Constraints

Buildings with flexible HVAC loads are spatially distributed, so the coordination strategy should satisfy power flow constraints, i.e., bus voltage and branch power flow limitations.

[1]While we assume DRG only outputs active power here, the proposed model can be readily extended to consider a DG's reactive power output.

The power flow in a distribution network can be described by the linearized DistFlow [30][2]:

$$\begin{cases} P_{ij,t} = \sum_{k\in\mathcal{C}_j} P_{jk,t} - p_{j,t} \\ Q_{ij,t} = \sum_{k\in\mathcal{C}_j} Q_{jk,t} - q_{j,t} \\ U_{j,t} = U_{i,t} - 2(r_{ij}P_{ij,t} + x_{ij}Q_{ij,t}) \\ \forall (i,j)\in\mathcal{B},\ \forall t\in\mathcal{T} \end{cases} \tag{10}$$

where $P_{ij,t}$ and $Q_{ij,t}$ are active and reactive power flows, respectively, on branch $(i,j)\in\mathcal{B}$; i and j are bus indexes, $i,j\in\mathcal{I}$; $p_{j,t}$ and $q_{j,t}$ are active and reactive power injections, respectively, at bus j; U_i is the square of the voltage at bus i; r_{ij} and x_{ij} are the resistance and reactance, respectively, of branch (i,j); and set $\mathcal{C}_j$ contains the child bus indexes of bus j, $\mathcal{C}_j\subseteq\mathcal{I}$. The net power at substation G_t^{g} is the summation of the active power flows from the slack bus ($i=0$) to its child buses, as follows:

$$G_t^{\mathrm{g}} = \sum_{j\in\mathcal{C}_0} P_{0j,t},\ \forall t\in\mathcal{T} \tag{11}$$

All bus voltages and branch power flows should lie in a proper range to ensure system security. According to (7) and (8), uncertainty $\boldsymbol{\xi}_t$ affects power injections on each bus. Based on linearized Distflow (10), this uncertainty further propagates to the square of the bus voltage $\boldsymbol{U}_t$, and branch power flows $\boldsymbol{P}_t$ and $\boldsymbol{Q}_t$. To maintain system security, a JCC is employed to manage the uncertainties:

$$\mathbb{P}\left(\begin{array}{l} U_{i,\min}\le U_{i,t}\le U_{i,\max},\ \forall i\in\mathcal{I} \\ P_{ij,t}^2+Q_{ij,t}^2\le (S_{ij}^{\max})^2,\ \forall (i,j)\in\mathcal{B} \end{array}\right)\ge 1-\epsilon \tag{12}$$

where $U_{i,\min}$ and $U_{i,\max}$ are the lower and upper bounds of the bus voltage; $S_{ij}^{\max}$ is the maximum allowable apparent power flow. Symbol ϵ is the risk parameter, which defines the maximum allowable probability of constraint violations.

Remark 1. Here, we use JCCs instead of individual ones to control the violation probability of all security constraints under the impacts of uncertainties from DRG. This is preferable in the coordination of DRG and HVAC loads because it can accurately ensure the security of the entire system with a predetermined confidence level.

4) Linearization of the Quadratic JCC

There are quadratic constraints inside the probability operator of (12), which are intractable. To address this issue, we introduce auxiliary variables $P_{ij,t}^{\mathrm{aux}}$ and $Q_{ij,t}^{\mathrm{aux}}$, and conservatively approximate each quadratic constraint inside the probability operator by

$$\begin{cases} (P_{ij,t}^{\mathrm{aux}})^2+(Q_{ij,t}^{\mathrm{aux}})^2\le (S_{ij}^{\max})^2 \\ |P_{ij,t}|\le P_{ij,t}^{\mathrm{aux}}, |Q_{ij,t}|\le Q_{ij,t}^{\mathrm{aux}} \end{cases} \quad \forall (i,j)\in\mathcal{B} \tag{13}$$

Note that $P_{ij,t}^{\mathrm{aux}}$ and $Q_{ij,t}^{\mathrm{aux}}$ are deterministic. Thus, the conic constraint, i.e., the first line of (13), does not contain any uncertainty. Then, by substituting (13), the quadratic JCC (12) can be approximated by a deterministic second-order cone constraint plus a linear JCC:

$$(P_{ij,t}^{\mathrm{aux}})^2+(Q_{ij,t}^{\mathrm{aux}})^2\le (S_{ij}^{\max})^2,\ \forall (i,j)\in\mathcal{B} \tag{14}$$

$$\mathbb{P}\left(\begin{array}{l} U_{i,\min}\le U_{i,t}\le U_{i,\max},\ \forall i\in\mathcal{I} \\ |P_{ij,t}|\le P_{ij,t}^{\mathrm{aux}}, |Q_{ij,t}|\le Q_{ij,t}^{\mathrm{aux}},\ \forall (i,j)\in\mathcal{B} \end{array}\right) \ge 1-\epsilon,\ \forall t\in\mathcal{T} \tag{15}$$

Obviously, any feasible solution of (15) must be feasible for (12). Hence (15) can guarantee the feasibility of solutions.

C. Optimization Problem

Our goal is to minimize the total cost. Thus, the optimization problem is formulated as:

$$\min_{(\boldsymbol{p}_t^{\mathrm{HV}},\boldsymbol{\lambda}_t,\boldsymbol{P}_t^{\mathrm{aux}},\boldsymbol{Q}_t^{\mathrm{aux}})_{\forall t\in\mathcal{T}}} \mathbb{E}\left(\sum_{t\in\mathcal{T}} EC_t\right) \tag{P1}$$

$$\text{s.t.}\ \ (1)\text{–}(11)\ \text{and}\ (14)\text{–}(15)$$

III. Learning-based Reformulation for Joint Chance Constraints

Constraint (15) is intractable because of the inside probability operator. We address this issue through a learning-based approach. We first propose a robust approximation for the JCC to eliminate the intractable probability operator. Then, an OC-SVC-based method is employed to construct a tight polyhedron uncertainty set for the previous robust approximation. A linear counterpart for the proposed OC-SVC-based uncertainty set is further developed to ensure computational tractability.

A. Robust Approximation of the JCC

Observing that all constraints inside the probability operator of (15) are linear, they can be expressed in a generic form

$$(\boldsymbol{H}_{m,t}\boldsymbol{\xi}_t)^{\mathrm{T}}\boldsymbol{y}_t\le b_{m,t}(\boldsymbol{y}_t),\ \forall m\in\mathcal{M},\ \forall t\in\mathcal{T} \tag{16}$$

where $\boldsymbol{H}_{m,t}$ and $\boldsymbol{\xi}_t$ are the coefficient matrix and random variable, respectively, in each constraint; $\boldsymbol{y}_t=[\boldsymbol{p}_t^{\mathrm{HV}},\boldsymbol{\lambda}_t,\boldsymbol{P}_t^{\mathrm{aux}},\boldsymbol{Q}_t^{\mathrm{aux}}]$ is the decision variable vector; $b_{m,t}$ is an affine function of $\boldsymbol{y}_t$; and $m\in\mathcal{M}=\{1,2,\cdots,M\}$ is the index of constraints inside the probability operator. By defining a new function $f_t(\boldsymbol{y}_t,\boldsymbol{\xi}_t)$ as:

$$f_t(\boldsymbol{y}_t,\boldsymbol{\xi}_t)=\max_{m\in\mathcal{M}}((\boldsymbol{H}_{m,t}\boldsymbol{\xi}_t)^{\mathrm{T}}\boldsymbol{y}_t-b_{m,t}(\boldsymbol{y}_t)),\ \forall t\in\mathcal{T} \tag{17}$$

Equation (15) can be expressed as:

$$\mathbb{P}(f_t(\boldsymbol{y}_t,\boldsymbol{\xi}_t)\le 0)\ge 1-\epsilon,\ \forall t\in\mathcal{T} \tag{18}$$

If we can find an uncertainty set $\mathcal{U}_t$ satisfying

$$\mathbb{P}(\boldsymbol{\xi}_t\in\mathcal{U}_t)\ge 1-\epsilon,\ \forall t\in\mathcal{T} \tag{19}$$

the intractable JCC (18) can be approximately expressed by a robust constraint,

$$\max_{\boldsymbol{\xi}_t\in\mathcal{U}_t}(f_t(\boldsymbol{y}_t,\boldsymbol{\xi}_t))\le 0,\ \forall t\in\mathcal{T} \tag{20}$$

and the probability operator can be eliminated. Obviously, the key problem of this robust approximation is to find an appropriate $\mathcal{U}_t$, which should satisfy feasibility, optimality, and tractability requirements:

[2]The linearized DistFlow model is an approximation of power flow equations, so it may introduce approximation errors. Nevertheless, reference [31] pointed out that this approximation error is usually small and will not affect the results significantly (e.g., if the maximum allowable voltage deviation is 5%, then the maximum relative error is only 0.25%).

1) Feasibility: $\mathcal{U}_t$ must cover at least $100(1-\epsilon)\%$ of samples in the historical dataset, i.e., (19);

2) Optimality: The space covered by $\mathcal{U}_t$ should be small, so that the obtained solution can achieve desirable energy efficiency;

3) Tractability: The robust approximation (20) with $\mathcal{U}_t$ as its uncertainty set must have a tractable counterpart so it can be effectively handled by off-the-shelf solvers.

B. OC-SVC-based Uncertainty Set

We leverage a popular learning-based anomaly detection method, one-class support vector clustering (OC-SVC), to construct the appropriate uncertainty set $\mathcal{U}_t$ [32]. For convenience, we omit the subscript t in this section. The idea of OC-SVC is to find a minimal sphere in high-dimension feature space as the boundary to separate normal and abnormal data, which can be expressed as:

$$\min_{R,\boldsymbol{o},\boldsymbol{\omega}} R^2 + \frac{1}{N\epsilon}\sum_{n\in\mathcal{N}}\omega_n \tag{P-SVC}$$

$$\text{s.t. } \|\boldsymbol{\psi}(\boldsymbol{\xi}^{(n)}) - \boldsymbol{o}\|^2 \le R^2 + \omega_n,\ \forall n\in\mathcal{N} \tag{21}$$

$$\omega_n \ge 0,\ \forall n\in\mathcal{N} \tag{22}$$

where R is the radius of the sphere; ϵ is a controllable parameter; $\boldsymbol{\psi}(\cdot)$ is a mapping function from the original space to high-dimensional feature space; $\boldsymbol{o}$ is the center of the sphere; and ω_n is a slack variable. The second term in the objective function is the penalty for outliers. By introducing dual variables $\boldsymbol{\alpha}$ and $\boldsymbol{\beta}$ for (21) and (22), the KKT conditions of P-SVC are

$$\mathbf{1}^{\mathrm{T}}\boldsymbol{\alpha} = 1,\ \boldsymbol{o} = \sum_{n\in\mathcal{N}}\alpha_n\boldsymbol{\phi}(\boldsymbol{\xi}^{(n)}),\ \boldsymbol{\alpha}+\boldsymbol{\beta} = \frac{1}{N\epsilon}\cdot\mathbf{1} \tag{23}$$

$$\omega_n\beta_n = 0,\ \forall n\in\mathcal{N} \tag{24}$$

$$\alpha_n(R^2 + \omega_n - \|\boldsymbol{\phi}(\boldsymbol{\xi}^{(n)}) - \boldsymbol{o}\|^2) = 0,\ \forall n\in\mathcal{N} \tag{25}$$

where (23) is obtained by setting the derivative of the Lagrangian function to zero, and (24) and (25) represent complementary slackness. Based on the previous KKT conditions, we can recognize interiors, boundaries, and outliers, as shown in Table I. We refer to samples on the boundary as boundary support vectors, and regard outliers and boundary support vectors as support vectors. The sets of support vectors and boundary support vectors are defined based on Table I:

$$\text{SV} = \{n \mid \alpha_n > 0,\ \forall n\in\mathcal{N}\} \tag{26}$$

$$\text{BSV} = n \mid 0 < \alpha_n < 1/(N\epsilon),\ \forall n\in\mathcal{N}\} \tag{27}$$

TABLE I
CLASSIFICATION OF SAMPLES

Dual variables of samples	Positions	Categories
$\alpha_n = 0$ $\beta_n = 1/(N\epsilon)$	$\|\boldsymbol{\phi}(\boldsymbol{\xi}^{(n)}) - \boldsymbol{o}\|^2 < R^2$	Interiors
$0 < \alpha_n < 1/(N\epsilon)$ $0 < \beta_n < 1/(N\epsilon)$	$\|\boldsymbol{\phi}(\boldsymbol{\xi}^{(n)}) - \boldsymbol{o}\|^2 = R^2$	Boundaries
$\alpha_n = 1/(N\epsilon)$ $\beta_n = 0$	$\|\boldsymbol{\phi}(\boldsymbol{\xi}^{(n)}) - \boldsymbol{o}\|^2 > R^2$	Outliers

Note that the solutions of $\boldsymbol{\alpha}$ and $\boldsymbol{\beta}$ can be obtained by solving the dual problem of P-SVC, as follows:

$$\min_{\boldsymbol{\alpha}} \sum_{n\in\mathcal{N}}\sum_{m\in\mathcal{N}}\alpha_n\alpha_m K(\boldsymbol{\xi}^{(n)},\boldsymbol{\xi}^{(m)}) - \sum_{n\in\mathcal{N}} K(\boldsymbol{\xi}^{(n)},\boldsymbol{\xi}^{(m)}) \tag{D-SVC}$$

$$\text{s.t. } 0 \ge \alpha_n \ge \frac{1}{N\epsilon},\ \forall n\in\mathcal{N} \tag{28}$$

$$\sum_{n\in\mathcal{N}}\alpha_n = 1 \tag{29}$$

where $K(\boldsymbol{\xi}^{(n)},\boldsymbol{\xi}^{(m)}) = \boldsymbol{\psi}(\boldsymbol{\xi}^{(n)})^{\mathrm{T}}\boldsymbol{\psi}(\boldsymbol{\xi}^{(m)})$ is the kernel function. This paper employs the weighted generalized intersection kernel [32] as our kernel function,

$$K(\boldsymbol{\xi}^{(1)},\boldsymbol{\xi}^{(2)}) = \sum_{d\in\mathcal{D}} l_d - \|\boldsymbol{W}(\boldsymbol{\xi}^{(1)} - \boldsymbol{\xi}^{(2)})\|_1 \tag{30}$$

where $\mathcal{D} = \{1, 2, \cdots, D\}$ is the dimension index set of $\boldsymbol{\xi}^{(1)}$ or $\boldsymbol{\xi}^{(2)}$; $l_d = \xi_{d,\max} - \xi_{d,\min}$, where $\xi_{d,\max}$ and $\xi_{d,\min}$ are the upper and lower bounds, respectively, of $\boldsymbol{\xi}$ in the d-th dimension; and $\boldsymbol{W} = \boldsymbol{\Sigma}^{-1/2}$, where $\boldsymbol{\Sigma}$ is the covariance matrix of the historical samples. Note that $K(\boldsymbol{\xi},\boldsymbol{\xi}) = \sum_{d\in\mathcal{D}} l_d$ is a constant.

Proposition 1. The OC-SVC-based uncertainty set, i.e., $\mathcal{U} = \|\boldsymbol{\phi}(\boldsymbol{\xi}^{(n)}) - \boldsymbol{o}\|^2 \le R^2$, can be expressed as a polyhedron in the original space of uncertainty $\boldsymbol{\xi}$, as follows:

$$\mathcal{U} = \left\{ \boldsymbol{\xi} \;\middle|\; \begin{array}{l} \exists \boldsymbol{\upsilon}_n \in \mathbb{R}^D,\ \forall n\in\text{SV}, \text{s.t.} \\ \displaystyle\sum_{n\in SV}\alpha_n\boldsymbol{\upsilon}_n^{\mathrm{T}}\mathbf{1} \le \gamma \\ -\boldsymbol{\upsilon}_n \le \boldsymbol{W}(\boldsymbol{\xi} - \boldsymbol{\xi}^{(n)}) \le \boldsymbol{\upsilon}_n,\ \forall n\in\text{SV} \end{array} \right\} \tag{31}$$

where $\boldsymbol{\upsilon}_n$ is an auxiliary variable. Parameter γ is equal to $\sum_{n\in\text{SV}}\alpha_n\|\boldsymbol{W}(\boldsymbol{\xi}^{(k)} - \boldsymbol{\xi}^{(n)})\|_1$ for any $k\in\text{BSV}$.

Proof: see Appendix A.

As mentioned above, a desirable uncertainty set must satisfy feasibility, optimality, and tractability requirements. We show that the OC-SVC-based uncertainty set can meet the feasibility requirement.

Proposition 2. The uncertainty set $\mathcal{U}$ defined in (31) can cover at least $100(1-\epsilon)\%$ of samples.

Proof: From Table I, we know that any outlier must have $\alpha_n = 1/(N\epsilon)$. If the number of outliers exceeds $N\epsilon$, then $\mathbf{1}^{\mathrm{T}}\boldsymbol{\alpha} > 1$ ($\alpha_n \ge 0$ for all samples), which conflicts with KKT condition (23). Hence the number of outliers must be no larger than $N\epsilon$, and the proposed uncertainty set can cover at least $100(1-\epsilon)\%$ of samples.

We verify the optimality performance of the proposed uncertainty set based on numerical experiments in section IV.

Since $\mathcal{U}$ is a polyhedron, we can find a linear counterpart for it, as we next discuss. Hence the tractability requirement can also be satisfied. This tractability requirement is also the main reason for choosing weighted generalized intersection as our kernel function. In fact, many other kernels, e.g., radial basis function, can also be applied to OC-SVC [33]. However, they may lead to non-convex uncertainty sets. As a result, it is hard to find a tractable counterpart when other kernel functions are employed.

C. Linear Robust Counterpart

We develop a linear counterpart for the robust approximation (20) to make the whole problem tractable. First, based on (17), robust approximation (20) can be expressed as:

$$\begin{aligned}&\max_{\boldsymbol{\xi}_t\in\mathcal{U}_t}\left\{\max_{\forall m\in\mathcal{M}}((\boldsymbol{H}_{m,t}\boldsymbol{\xi}_t)^{\mathrm{T}}\boldsymbol{y}_t-b_{m,t}(\boldsymbol{y}_t))\right\}\le 0\\&\Leftrightarrow\max_{\boldsymbol{\xi}_t\in\mathcal{U}_t}\left((\boldsymbol{H}_{m,t}\boldsymbol{\xi}_t)^{\mathrm{T}}\boldsymbol{y}_t\right)\le b_{m,t}(\boldsymbol{y}_t),\ \forall m\in\mathcal{M}\end{aligned}\tag{32}$$

Based on the following proposition, we can find a linear counterpart for the robust constraint (32).

Proposition 3. If the uncertainty set is defined by (31), then (32) can be reformulated as linear constraints,

$$\begin{cases}\sum_{n\in\mathrm{SV}_t}(\boldsymbol{\mu}_{n,m,t}-\boldsymbol{\rho}_{n,m,t})^{\mathrm{T}}\boldsymbol{W}_t\boldsymbol{\xi}_t^{(n)}+\pi_{m,t}\gamma_t\le b_{m,t}\\\sum_{n\in\mathrm{SV}_t}\boldsymbol{W}_t(\boldsymbol{\rho}_{n,m,t}-\boldsymbol{\mu}_{n,m,t})+\boldsymbol{H}_{m,t}^{\mathrm{T}}\boldsymbol{y}_t=\boldsymbol{0}\\\boldsymbol{\rho}_{n,m,t}+\boldsymbol{\mu}_{n,m,t}=\pi_{m,t}\alpha_{n,t}\boldsymbol{1},\ \pi_{m,t}\ge 0\\\boldsymbol{\mu}_{n,m,t},\boldsymbol{\rho}_{n,m,t}\in\mathbb{R}_+^D,\ \forall n\in\mathrm{SV}_t,\ \forall m\in\mathcal{M},\ \forall t\in\mathcal{T}\end{cases}\tag{33}$$

where $\boldsymbol{\rho}_{n,m,t}$, $\boldsymbol{\mu}_{n,m,t}$, and $\pi_{m,t}$ are Lagrange multipliers for the m-th constraint at time t in (32).

Proof: see Appendix B.

D. Summary

Based on the previous linear counterpart, we can reformulate problem P1 as:

$$\min_{\boldsymbol{y}_t,\ \forall t\in\mathcal{T}}\sum_{t\in\mathcal{T}}\mathbb{E}\left(\sum_{t\in\mathcal{T}}EC_t\right)\tag{P2}$$

$$\text{s.t.}\quad (1)\text{–}(4),\ (5)\text{–}(11),\ (7)\text{–}(9),\ (14),\ \text{and}\ (33)$$

Figure 1 summarizes the procedure to convert intractable JCCs to tractable linear constraints. We develop a robust optimization-based approximation (20) for the original JCC (15), and solve the dual problem D-SVC to find support vectors and construct the OC-SVC-based uncertainty set (31). We implement the linear counterpart based on (33) to replace the original intractable JCC, and solve problem P2 to obtain the optimal schedule of HVAC systems and DRG.

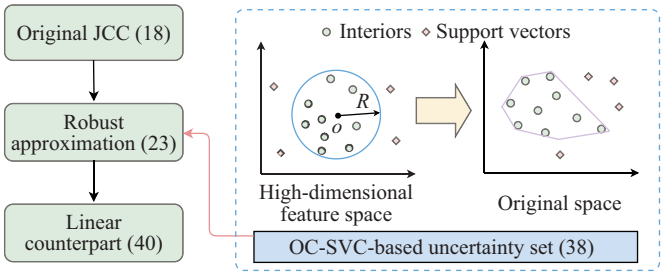

Fig. 1. The whole procedure for converting JCCs into linear constraints.

Although this paper only involves the uncertainties from DRG, the proposed model can readily consider uncertainties from other sources. For example, if power demands are uncertain, then p_t^{e} and q_t^{e} in (7)–(8) need to be treated as new uncertain parameters. Nevertheless, constraints inside the probability operator of the JCC (12) are still linear. As a result, we can directly use the proposed model to construct a linear counterpart for this JCC.

IV. Case Study

A. Simulation Set Up

We describe a case study based on the IEEE 13-bus system with wind turbines DRG1 and DRG2 to provide DRG, as shown in Fig. 2(a). The network parameters (e.g., branch resistance and reactance) can be found on the IEEE website [34]. The indoor heat loads and base power demands (i.e., demands except HVAC loads) in different nodes are illustrated in Fig. 2(b)–(d). The unit prices for purchasing and selling electricity are shown in Fig. 3(a), and Fig. 3(b) shows the nominal outputs of DRG and outdoor temperature. The optimization horizon is set as 24h, and the time interval is one hour. Other parameters can be found in Table II. Because the forecasting errors of wind generation can be variant,

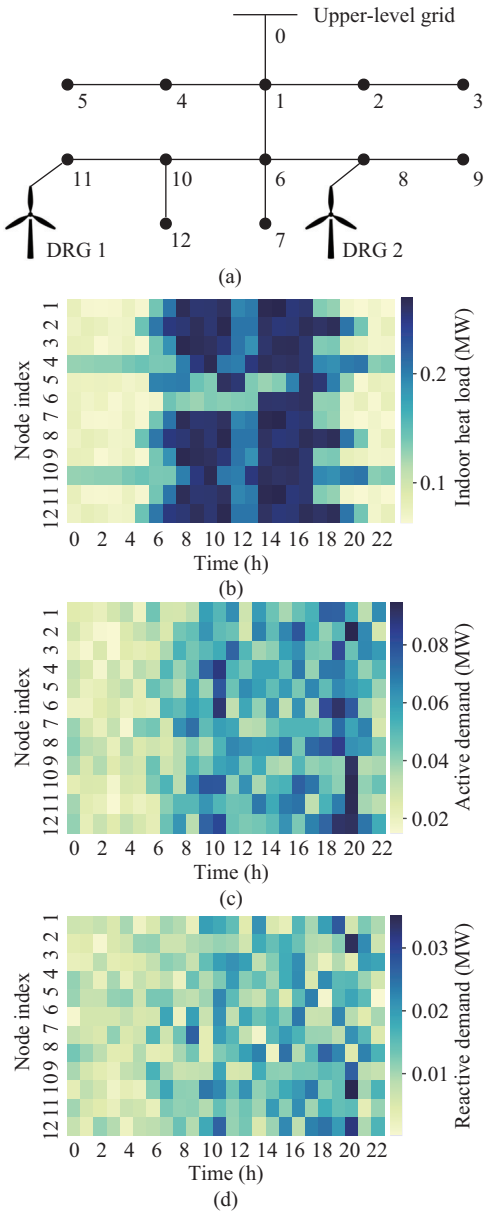

Fig. 2. The test system and parameters used in the case study. (a) The 13-Bus test system, (b) indoor heat loads. (c) Base active power demands. (d) Base reactive power demands. In (a), symbols "DRG1" and "DRG2" represent two distributed renewable generators.

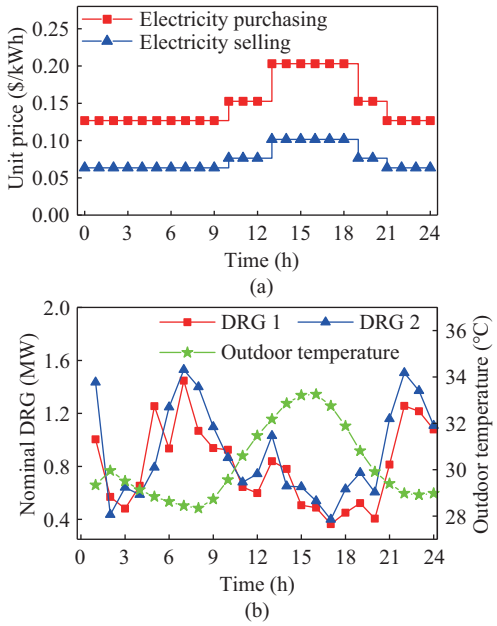

Fig. 3. (a) Unit prices of electricity purchasing and selling and (b) nominal outputs of DRG and outdoor temperature.

TABLE II
PARAMETERS IN CASE STUDY

Parameters	Value	Parameters	Value
C_i	1 MWh/°C	$\overline{p}_i$	0.5 MW
R_i	20 °C/MW	ϕ_i	0.98
COP_i	3.6	$U_{i,\min}$	0.95 p.u.
$\underline{\theta}_i$	24 °C	$U_{i,\max}$	1.05 p.u.
$\overline{\theta}_i$	28 °C	$S_{ij,t}$	2 MW

we implement Cases 1–3 with samples generated by Beta, Weibull, and Gaussian distributions, respectively, to simulate the historical data. The generated data has been uploaded on [35].

All numerical experiments are tested on an Intel 8700 3.20-GHz CPU with 16 GB memory. GUROBI and CVXPY are employed to solve the optimization problem.

B. Benchmarks

We introduce three models as benchmarks:

1) B1(SA+Box): Scenario approach combined with a box uncertainty set [24], [25];
2) B2(SA+CH): Scenario approach combined with a convex hull uncertainty set [27];
3) B3(Bonferroni): Bonferroni approximation, which approximates the original JCC with multiple ICCs [20][3].

We also test the performance of SAA. However, since it requires multiple constraints for every historical sample, out-of-memory issue occurs, which implies a huge computational burden. Parameters used in simulations are consistent among all methods, so results can be compared.

[3]The uncertainties in ICCs may not be normally distributed. In order to guarantee feasibility, we employ the moment-based distributionally robust chance constrained method used in [16] to reformulate these ICCs as second-order cone constraints.

C. Computational Cost of the Learning Step

The proposed model is based on a trained OC-SVC model, and the training process is implemented by scikit-learn, a famous machine-learning library for Python [36]. Fig. 4 summarizes the time spent on this learning step in different cases. Because OC-SVC is a mature machine learning model, it can be trained well in a short time. In all cases, the time spent on learning is less than 10 s. Moreover, this learning step can be conducted offline because it requires no real-time demand information. Hence, it does not affect the computational efficiency of real-time scheduling.

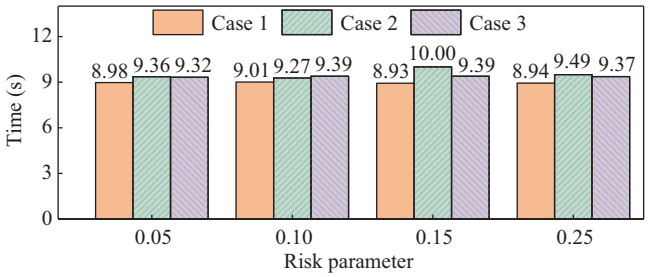

Fig. 4. Time spent on the learning step in different cases.

D. Case 1: Beta Distributed Uncertainties

1) Shape of Uncertainty Sets

Figure 5 illustrates the shapes of uncertainty sets constructed by different models based on the samples at $t = 6$ in Case 1. Since the scenarios are randomly drawn, some extreme samples are chosen. Hence, the uncertainty sets of scenario approach-based models B1 and B2 must be large enough to cover these extreme samples, which is unnecessarily conservative. Unlike B1 and B2, the proposed model introduces OC-SVC to decide which samples must be covered. By solving P-VC, samples that are far from the majority of samples can be recognized as outliers. Compared to B1 and B2, samples covered by the proposed uncertainty set are more concentrated, and the proposed uncertainty set (bounded by the green cross in Fig. 5) is much smaller. These results indicate that the proposed model can achieve better optimality than B1 and B2.

2) Optimality, Feasibility and Time-efficiency

Figure 6 summarizes the energy cost, average utilization rate of DRG, solution time, and maximum violation probability obtained by different models. The energy cost of Bonferroni approximation B3 is the worst among all models because the number of constraints in the original JCC (15) is relatively large, and the risk parameter of each ICC is too small (less than 0.0015), leading to a conservative solution. The proposed model achieves the lowest energy cost and highest utilization rate of DRG. The proposed OC-SVC-based uncertainty set can cover the historical samples more tightly than conventional box and convex hull uncertainty sets. Hence the solution is less conservative (i.e., the energy cost is smaller), and more DRG can be utilized in distribution networks; e.g., the average utilization rate of DRG obtained by the proposed model is around 2.5% and 1.5% higher than in B1 and B2, respectively. These results confirm that the proposed model can better promote DRG utilization.

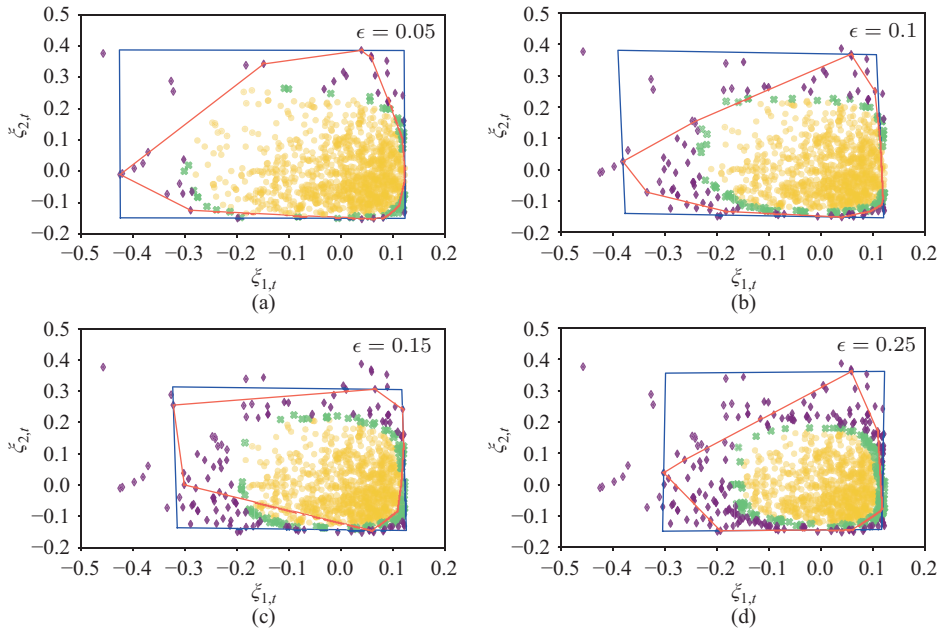

Fig. 5. Uncertainty sets in Case 1 (uncertainties follow Beta distribution) generated by different models at $t = 6$: (a) $\epsilon = 0.05$; (b) $\epsilon = 0.10$; (c) $\epsilon = 0.15$; (d) $\epsilon = 0.25$. Blue rectangle and red polyhedron indicate uncertainty sets constructed by B1(SA+Box) and B2(SA+CH), respectively. SVC-based uncertainty set is formed by boundary support vectors (green points). Internal samples and outliers are marked as gold dots and purple diamonds, respectively.

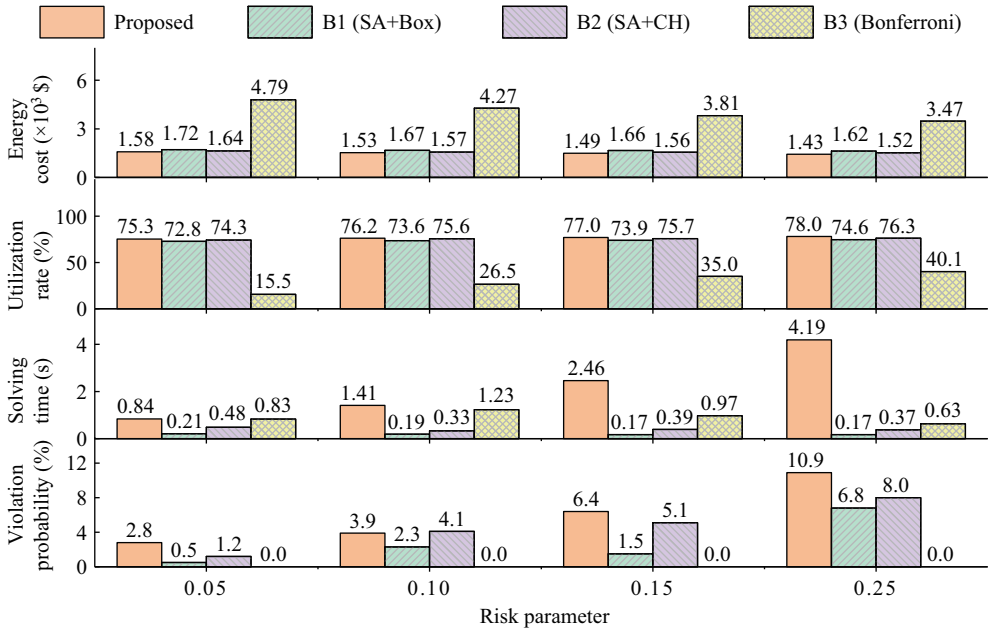

Fig. 6. Results of energy costs, average utilization rates of DRG, solving times, and maximum violation probabilities obtained by different models in Case 1 (Uncertainties follow the Beta distribution).

The solving time of the proposed model is always larger than those of B1–B3 because it needs to introduce more constraints. According to (33), the proposed model needs to introduce $|\mathcal{M}| \cdot |\mathrm{SV}_t|$ constraints for each JCC. The value of $|\mathcal{M}| \cdot |\mathrm{SV}_t|$ is relatively large, so the corresponding computational burden is high. Conversely, since our test system only contains two renewable generators, the dimension number of the uncertainty vector is low, resulting in a relatively small scenario number in B1 and B2 [24], [25]. Thus, a simple uncertainty set can cover all these scenarios, so counterparts of B1 and B2 only contain a small number of constraints. B3 approximates the original JCC into multiple ICCs, and the number of ICCs is equal to $|\mathcal{M}|$, which is much smaller than that in the proposed model. As a result, the computational efficiency of the proposed model is the worst. Nevertheless, the maximum solving time of the proposed model is only around 4 s. Given that the optimization horizon is 24h, this computational efficiency is acceptable. Moreover, its solving time decreases with the risk parameter's decrease. Obviously, if the risk parameter is small, then only a few samples of

uncertainties are allowed to violate constraints. In this case, the support vector number $|\mathrm{SV}_t|$ is also small. As a result, only a few constraints are introduced, resulting in a lower computational burden. For example, when $\epsilon = 0.05$, it can complete the solution process in 1 s. Considering that the risk parameter is commonly maintained at a low level, the proposed model can meet the computational efficiency requirements well in practice.

The violation probabilities of the original JCC (15) obtained by all models, including the proposed one, are always lower than the given risk parameter. For B1–B3, it has been pointed out [10] that they provide conservative approximations for JCCs. Equations (18)–(20) imply that the proposed model is also an inner approximation. Hence all four models can guarantee feasible solutions.

E. Case 2: Weibull Distributed Uncertainties

1) Shape of Uncertainty Sets

Figure 7 shows the uncertainty sets established by different models in Case 2. Similar to Case 1, the proposed OC-SVC-based method can capture the characteristics of the Weibull distribution and tightly cover most samples. Therefore, the unnecessary space introduced by the proposed uncertainty set is smaller than those of scenario approaches B1 and B2.

2) Optimality, Feasibility and Time-efficiency

The results of different models in Case 2 are listed in Fig. 8. Bonferroni approximation B3 shows the worst energy efficiency because of the small risk parameter in each ICC. With the smallest volume of the OC-SVC-based uncertainty set, the proposed model achieves the highest energy efficiency and utilization rate of DRG with proper feasibility.

F. Case 3: Normally Distributed Uncertainties

1) Shape of Uncertainty Sets

Figure 9 presents results of uncertainty sets constructed by different models with normally distributed uncertainties. Similar to Cases 1 and 2, the proposed uncertainty set has the smallest volume. The other two are relatively large because they must cover some extreme samples (such as at the bottom-right corner).

2) Optimality, Feasibility and Time-efficiency

Figure 10 summarizes the energy cost, average utilization rate of DRG, solution time, and maximum violation probability. The energy cost of the proposed model is the lowest, e.g., 13.4%, 4.2%, and 66.4% less than those of B1–B3, respectively, with risk parameter $\epsilon = 0.05$. Its utilization rate of DRG is also the highest, e.g., 4.9%, 1.7%, and 59.4% higher than those of B1–B3, respectively, at $\epsilon = 0.05$. Although its solution time is greater, the computational efficiency is still acceptable.

The results in Cases 1–3 also confirm that the proposed model can handle JCCs with arbitrarily distributed uncertainties, confirming its generalization performance.

G. Effectiveness Under Correlated Uncertainties

In practice, the outputs of DRG in one distribution network may be correlated. This correlation shall be properly considered because it may significantly affect the decision of power scheduling [37]. In fact, this correlation can help eliminate many unlikely-to-happen scenarios and improve the accuracy of uncertainty sets [38]. Since the proposed model constructs the uncertainty set based on historical samples, it can easily capture this correlation. As a result, the proposed model can also be applied to cases with correlated uncertainties.

To better verify the effectiveness of the proposed model, we further implement a case with correlated uncertainties. Specifically, this case assumes that the uncertainties from the DRG1 and DRG2 in Fig. 2(a) follow a joint Gaussian distribution. Expectation $\boldsymbol{\mu}$ and covariance $\mathbf{Cov}$ of this joint distribution are expressed as (34):

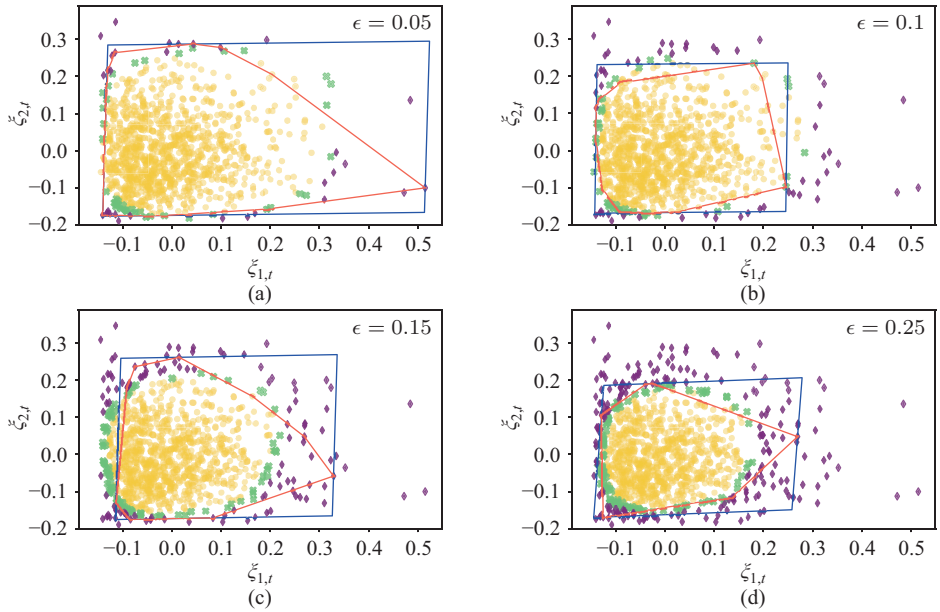

Fig. 7. Uncertainty sets generated by different models in Case 2 (uncertainties follow Weibull distribution) at $t = 6$: (a) $\epsilon = 0.05$; (b) $\epsilon = 0.10$; (c) $\epsilon = 0.15$; (d) $\epsilon = 0.25$.

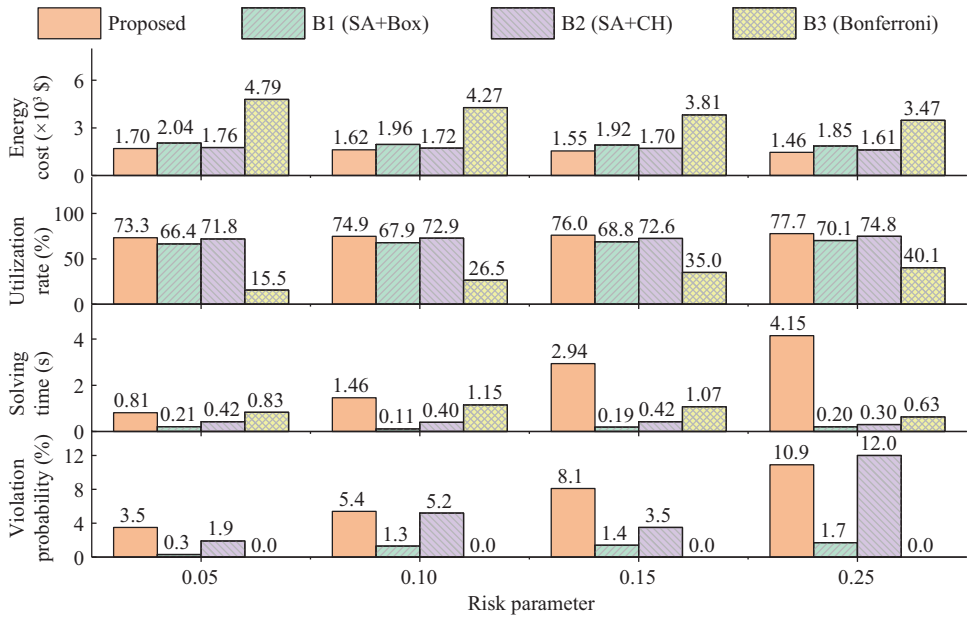

Fig. 8. Results of energy costs, average utilization rates of DRG, solution times, and maximum violation probabilities obtained by different models in Case 2 (uncertainties follow Weibull distribution).

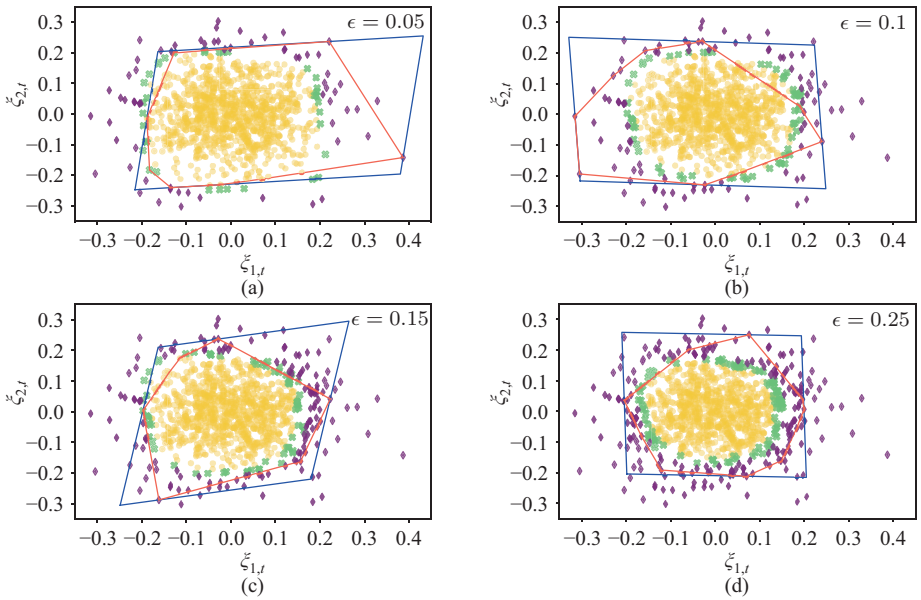

Fig. 9. Uncertainty sets generated by different models in Case 3 (uncertainties follow a Gaussian distribution) at $t = 6$: (a) $\epsilon = 0.05$; (b) $\epsilon = 0.10$; (c) $\epsilon = 0.15$; (d) $\epsilon = 0.25$.

$$\boldsymbol{\mu} = (0, 0), \ \mathbf{Cov} = \begin{bmatrix} 0.01 & 0.008 \\ 0.008 & 0.01 \end{bmatrix} \tag{34}$$

B1–B3 are also introduced as benchmarks for comparison. Since the uncertainties here are normally distributed, we use the widely used second-order cone reformulation for the chance constraints with Gaussian uncertainties to handle each ICC [10].

Figure 11 illustrates shapes of uncertainty sets constructed by different models based on samples at $t = 6$ in the case with correlated uncertainties. Similar to Caes 1–3, the uncertainty sets of B1 and B2 must be large enough to cover these extreme samples. Conversely, the proposed uncertainty set can cover most samples more tightly, so it is the smallest one, which indicates its desirable optimality.

Figure 12 summarizes the energy cost, average utilization rate of DRG, solution time, and maximum violation probability obtained by different models. B3 always derives the highest energy cost and lowest utilization rate of distributed renewable generation (DRG) among all models because the risk parameter in each ICC is very small. The proposed model achieves the lowest energy cost and highest utilization rate of DRG because its uncertainty set is the smallest. Although its computational performance is worse than other models, the maximum solving time is only 2.93 s, which is acceptable in practice. All four models, including the proposed one, can guarantee feasibility because all of them are based on

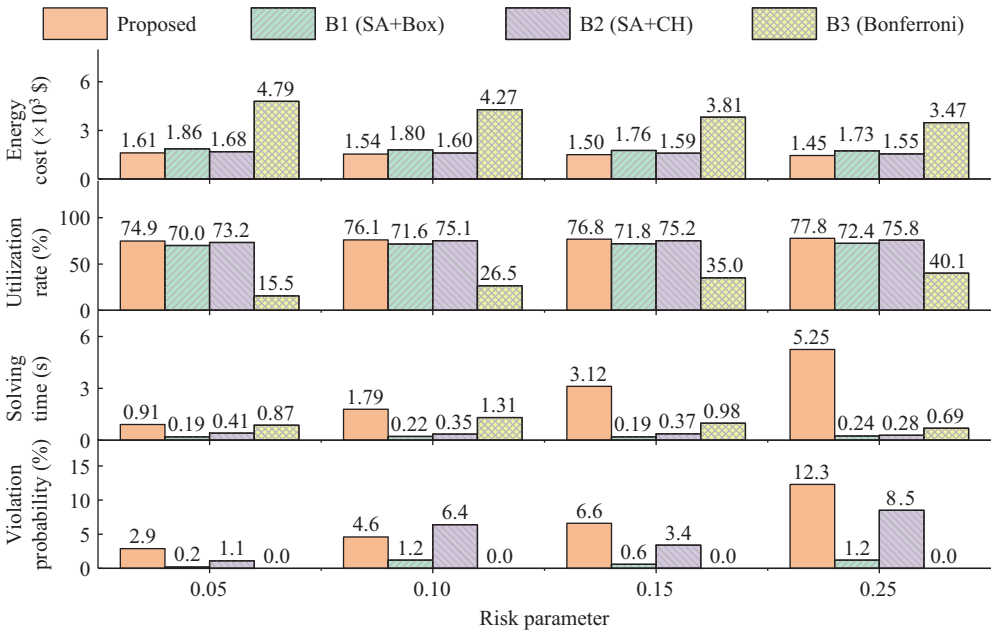

Fig. 10. Results of energy costs, average utilization rates of DRG, solution times, and maximum violation probabilities obtained by different models in **Case 3** (uncertainties follow a Gaussian distribution).

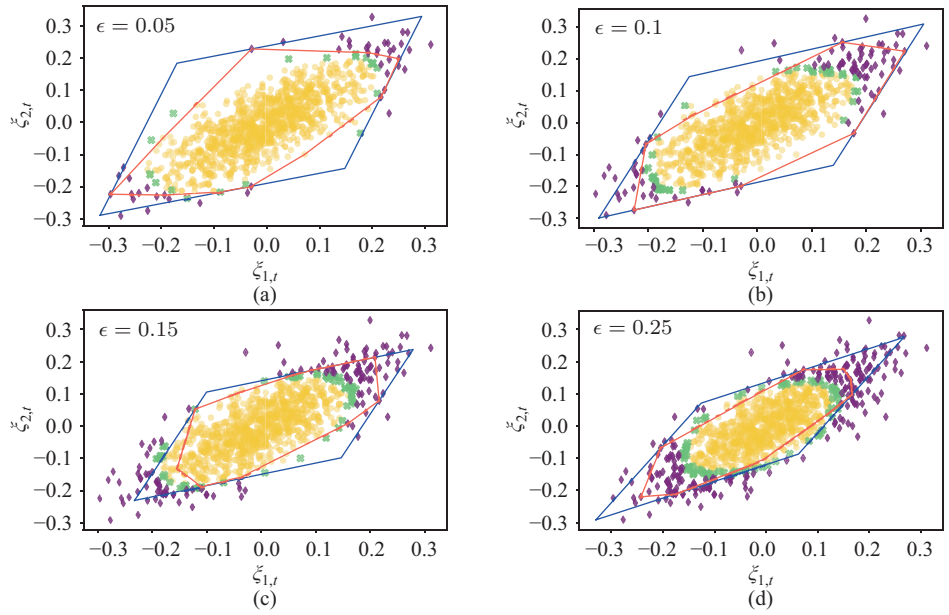

Fig. 11. Uncertainty sets generated by different models at $t = 6$ in the case with correlated uncertainties: (a) $\epsilon = 0.05$; (b) $\epsilon = 0.10$; (c) $\epsilon = 0.15$; (d) $\epsilon = 0.25$.

inner approximations of the intractable JCC. These results confirm the proposed model can achieve desirable optimality and feasibility with guaranteed computational efficiency.

H. Effectiveness Under Heterogeneous Parameters

In Cases 1–3, we assume that the building parameters of all nodes are homogeneous. To better verify the performance of the proposed model, we implement a case study in which different nodes have heterogeneous parameters. Fig. 13 shows the heat capacity C_i of the building, thermal resistance R_i between indoor and outdoor environments, coefficient of performance COP_i, and coefficient $\sqrt{(1-\phi_i^2)}/\phi_i$ used in (3). Buildings connected to different nodes obviously have heterogeneous parameters and various demands.

Figure 14 summarizes the results of this case study. Even with some heterogeneity in the parameters, the proposed model achieves the highest energy efficiency and utilization rate of DRG. Moreover, the violation probability of the JCC is always less than the given risk parameter. Although the solution time is longer, the maximum solution time is only 3.36 s.

I. Effectiveness of Flexibility From HVAC Loads

Figure 15 shows indoor temperatures, total heating load (heat loads from indoor sources plus heat transfer from outdoor

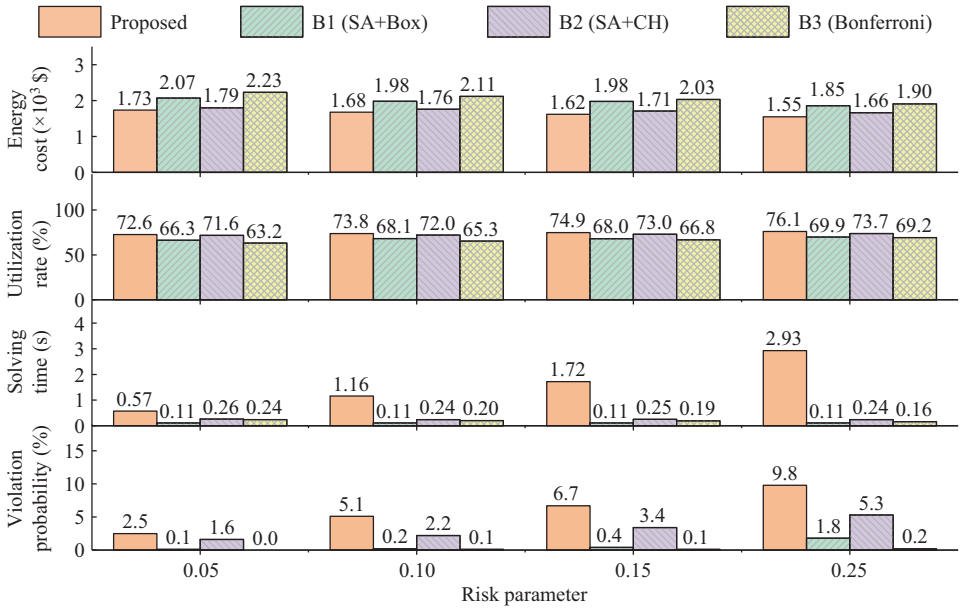

Fig. 12. Results of energy costs, average utilization rates of distributed renewable generation, solution times, and maximum violation probabilities obtained by different models in the case with correlated uncertainties.

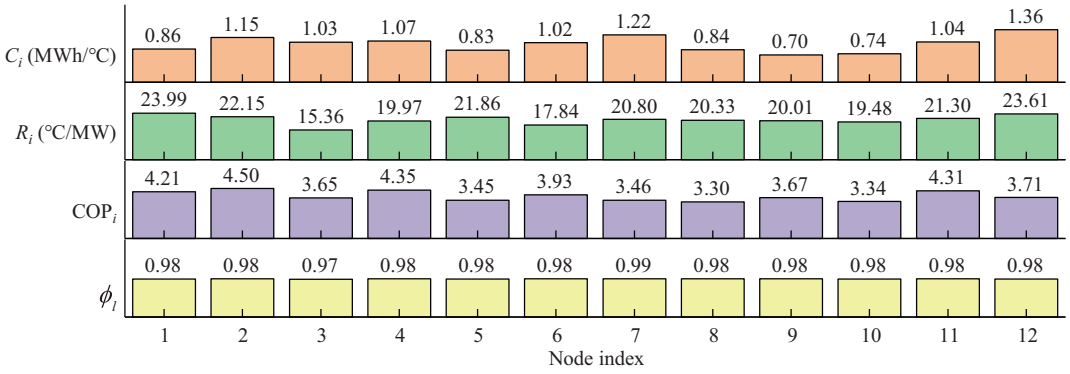

Fig. 13. The heterogeneous parameters in different nodes.

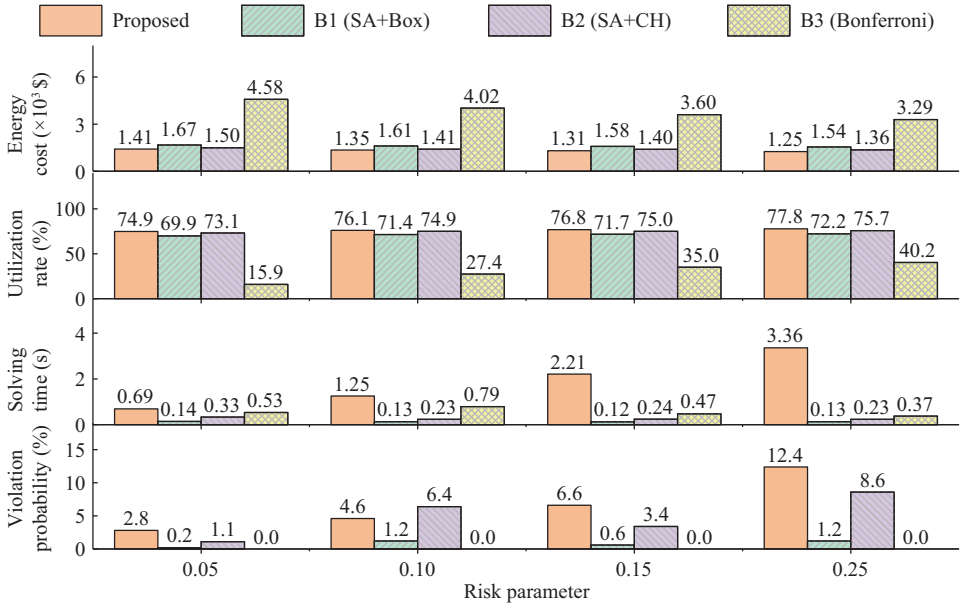

Fig. 14. Simulation results in the case with heterogeneous parameters.

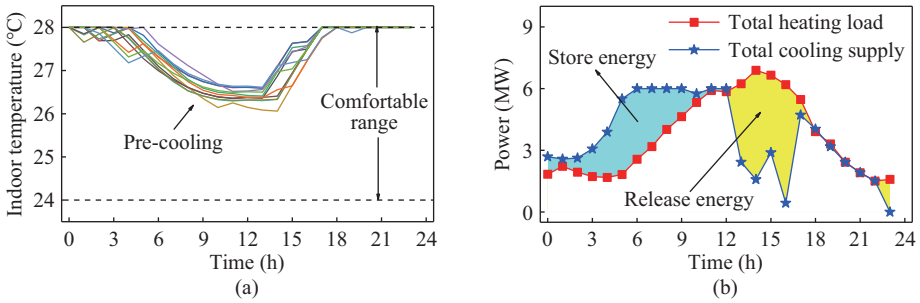

Fig. 15. Results of (a) indoor temperatures and (b) total heating load and cooling supply with Beta distributed uncertainties and $\epsilon = 0.05$.

environments), and cooling supply. The results are obtained by the proposed model with Beta distributed uncertainties with $\epsilon = 0.05$. During the period from 4:00 a.m. to 12:00 a.m., a significant temperature drop occurs in each building, which we refer to as pre-cooling, and the energy storage is based on this. During these hours, the available DRG power is relatively high, and the electricity price is low. To reduce the whole-day energy cost, the distribution network unlocks building thermal flexibility to store as much cooling power as possible for later use. Thus, the total cooling supply is much higher than the required total heating load during this period, as shown in Fig. 15(b). In the next few hours, the electricity price increases while the available DRG power decreases, and the stored cooling power is released. Therefore, the total cooling supply is visibly lower than the total heating load, leading to a noticeable increase in indoor temperatures. These results confirm that buildings can serve as batteries to provide operational flexibility for distribution networks.

Since the energy storage of buildings is based on pre-cooling, the variation of the lower bound of the indoor temperature, i.e., $\underline{\boldsymbol{\theta}}$, influences the capacity of the building's thermal flexibility. We change $\underline{\boldsymbol{\theta}}$ to verify the effectiveness of this flexibility, with results as shown in Fig. 16. With the growth of $\underline{\boldsymbol{\theta}}$, the capacity of the building thermal flexibility becomes smaller because less cooling power can be stored in indoor environments, leading to a lower utilization rate of DRG and higher energy cost.

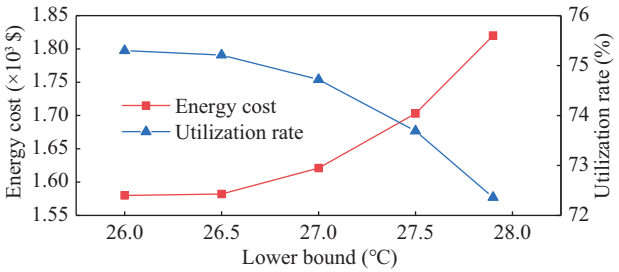

Fig. 16. Effects of temperature lower bound on energy cost and average utilization rate of DRG with $\epsilon = 0.05$.

V. Conclusion

This paper proposes a learning-based approach to promote DRG integration by scheduling flexible HVAC loads. Violation probabilities of all critical constraints are managed by JCCs to ensure the security of the whole system. To overcome the intractability of JCCs, this paper develops a robust constraint with a novel OC-SVC-based polyhedron uncertainty set to safely approximate JCCs. A linear counterpart was developed to guarantee computational efficiency. Numerical experiments on an IEEE 13-bus system indicated that the proposed uncertainty set can tightly cover most historical samples. Hence, the proposed model could achieve better optimality than the widely used scenario approach and Bonferroni approximation. Simulation results also confirm that the flexibility of HVAC loads can promote integration of DRG and enhance energy efficiency.

Appendix A

Proof of Proposition 1: According to Table I, the radius R is equal to the distance from the vector $\boldsymbol{o}$ to any boundary support vector,

$$R^2 = \|\boldsymbol{\phi}(\boldsymbol{\xi}^{(k)}) - \boldsymbol{o}\|^2, \ k \in \text{BSV} \tag{A1}$$

Based on (23), we can substitute $\boldsymbol{o} = \sum_{n\in\mathcal{N}} \alpha_n \boldsymbol{\phi}(\boldsymbol{\xi}^{(n)})$ in (A1) to obtain

$$R^2 = K(\boldsymbol{\xi}^{(k)}, \boldsymbol{\xi}^{(k)}) - 2\sum_{n\in\mathcal{N}} \alpha_n K(\boldsymbol{\xi}^{(k)}, \boldsymbol{\xi}^{(n)}) + \sum_{n\in\mathcal{N}}\sum_{m\in\mathcal{N}} \alpha_n\alpha_m K(\boldsymbol{\xi}^{(n)}, \boldsymbol{\xi}^{(m)}), \ k \in \text{BSV} \tag{A2}$$

Similarly, by substituting $\boldsymbol{o} = \sum_{n\in\mathcal{N}} \alpha_n \boldsymbol{\phi}(\boldsymbol{\xi}^{(n)})$, the region bounded by the minima sphere, i.e., $\{\boldsymbol{\xi} | \|\boldsymbol{\phi}(\boldsymbol{\xi}) - \boldsymbol{o}\|^2 \le R^2\}$, can be expressed as

$$\mathcal{U} = \left\{\boldsymbol{\xi} | K(\boldsymbol{\xi}, \boldsymbol{\xi}) - 2\sum_{n\in\mathcal{N}} \alpha_n K(\boldsymbol{\xi}, \boldsymbol{\xi}^{(n)}) + \sum_{n\in\mathcal{N}}\sum_{m\in\mathcal{N}} \alpha_n\alpha_m K(\boldsymbol{\xi}^{(n)}, \boldsymbol{\xi}^{(m)}) \le R^2\right\} \tag{A3}$$

Then, substituting (A2) and (30) in (A3), we can rewrite the uncertainty set as

$$\begin{aligned}\mathcal{U} &= \left\{\boldsymbol{\xi} | \sum_{n\in\mathcal{N}} \alpha_n K(\boldsymbol{\xi}, \boldsymbol{\xi}^{(n)}) \ge \sum_{n\in\mathcal{N}} \alpha_n K(\boldsymbol{\xi}^{(k)}, \boldsymbol{\xi}^{(n)})\right\} \\ &= \left\{\boldsymbol{\xi} | \sum_{n\in\text{SV}} \alpha_n \|\boldsymbol{W}(\boldsymbol{\xi} - \boldsymbol{\xi}^{(n)})\|_1 \le \gamma\right\}\end{aligned} \tag{A4}$$

where $\gamma = \sum_{n\in\text{SV}} \alpha_n \|\boldsymbol{W}(\boldsymbol{\xi}^{(k)} - \boldsymbol{\xi}^{(n)})\|_1$. By introducing auxiliary variable $\boldsymbol{\upsilon}_n$, the L1-norm operator can be eliminated, and $\mathcal{U}$ can be reformulated as (31) in Proposition 1.

APPENDIX B

Proof of Proposition 3: The LHS term in (32) is equivalent to the following linear programming problem:

$$\max_{\boldsymbol{\xi}_t, \boldsymbol{v}_{n,t}} (\boldsymbol{H}_{m,t}\boldsymbol{\xi}_t)^{\mathrm{T}}\boldsymbol{y}_t \tag{P-A1}$$

$$\text{s.t.} \quad \sum_{n\in \mathrm{SV}_t} \alpha_{n,t}\boldsymbol{v}_{n,t}^{\mathrm{T}}\mathbf{1} \le \gamma_t$$

$$-\boldsymbol{v}_{n,t} \le \boldsymbol{W}(\boldsymbol{\xi}_t - \boldsymbol{\xi}_t^{(n)}) \le \boldsymbol{v}_{n,t},\ \forall n \in \mathrm{SV}_t$$

By introducing Lagrange multipliers $\boldsymbol{\rho}_{n,t}$, $\boldsymbol{\mu}_{n,t}$, and π_t, we can obtain its dual problem:

$$\min_{\substack{\boldsymbol{\rho}_{n,m,t},\\ \boldsymbol{\mu}_{n,m,t},\\ \pi_{m,t}}} \sum_{n\in \mathrm{SV}_t} (\boldsymbol{\mu}_{n,m,t} - \boldsymbol{\rho}_{n,m,t})^{\mathrm{T}}\boldsymbol{W}_t\boldsymbol{\xi}_t^{(n)} + \pi_{m,t}\gamma_t \tag{D-A1}$$

$$\text{s.t.} \sum_{n\in \mathrm{SV}_t} \boldsymbol{W}_t(\boldsymbol{\rho}_{n,m,t} - \boldsymbol{\mu}_{n,m,t}) + \boldsymbol{H}_{m,t}^{\mathrm{T}}\boldsymbol{y}_t = \mathbf{0}$$

$$\boldsymbol{\rho}_{n,m,t} + \boldsymbol{\mu}_{n,m,t} = \pi_{m,t}\alpha_{n,t}\mathbf{1}$$

$$\pi_{m,t} \ge 0, \boldsymbol{\mu}_{n,m,t}, \boldsymbol{\rho}_{n,m,t} \in \mathbb{R}_+^D,\ \forall n \in \mathrm{SV}_t$$

Note that P-A1 is a linear problem, so the optimal solutions of P-A1 and D-A1 are equal based on strong duality. Finally, by substituting D-A1 in (32), Proposition 3 can be proved.

REFERENCES

[1] A. Ehsan, M. Cheng, and Q. Yang, "Scenario-based planning of active distribution systems under uncertainties of renewable generation and electricity demand," *CSEE Journal of Power and Energy Systems*, vol. 5, no. 1, pp. 56–62, Mar. 2019.

[2] S. Dalhues, Y. Zhou, O. Pohl, F. Rewald, F. Erlemeyer, D. Schmid, J. Zwartscholten, Z. Hagemann, C. Wagner, D. M. Gonzalez, H. Liu, M. M. Zhang, J. Y. Liu, C. Rehtanz, Y. Li, and Y. J. Cao, "Research and practice of flexibility in distribution systems: A review," *CSEE Journal of Power and Energy Systems*, vol. 5, no. 3, pp. 285–294, Sep. 2019.

[3] Y. Wang, Y. Tang, Y. Xu, and Y. L. Xu, "A distributed control scheme of thermostatically controlled loads for the building-microgrid community," *IEEE Transactions on Sustainable Energy*, vol. 11, no. 1, pp. 350–360, Jan. 2020.

[4] W. Mendieta and C. A. Cañizares, "Primary frequency control in isolated microgrids using thermostatically controllable loads," *IEEE Transactions on Smart Grid*, vol. 12, no. 1, pp. 93–105, Jan. 2021.

[5] R. L. Li and S. You, "Exploring potential of energy flexibility in buildings for energy system services," *CSEE Journal of Power and Energy Systems*, vol. 4, no. 4, pp. 434–443, Dec. 2018.

[6] G. Chen, B. Yan, H. C. Zhang, D. D. Zhang, and Y. H. Song, "Time-efficient strategic power dispatch for district cooling systems considering evolution of cooling load uncertainties," *CSEE Journal of Power and Energy Systems*, vol. 8, no. 5, pp. 1457–1467, Sep. 2022.

[7] J. Y. Wang, S. Huang, D. Wu, and N. Lu, "Operating a commercial building HVAC load as a virtual battery through airflow control," *IEEE Transactions on Sustainable Energy*, vol. 12, no. 1, pp. 158–168, Jan. 2021.

[8] Y. S. Sun, Z. X. Zhao, M. Yang, D. Q. Jia, W. Pei, and B. Xu, "Overview of energy storage in renewable energy power fluctuation mitigation," *CSEE Journal of Power and Energy Systems*, vol. 6, no. 1, pp. 160–173, Mar. 2020.

[9] X. C. Li, Y. X. Liu, L. Guo, X. L. Li, and C. S. Wang, "Data-driven based uncertainty set modeling method for microgrid robust optimization with correlated wind power," *CSEE Journal of Power and Energy Systems*, vol. 9, no. 2, pp. 420–432, Mar. 2023.

[10] X. B. Geng and L. Xie, "Data-driven decision making in power systems with probabilistic guarantees: Theory and applications of chance- constrained optimization," *Annual Reviews in Control*, vol. 47, pp. 341–363, May 2019.

[11] Z. N. Wei, J. Sun, Z. J. Ma, G. Q. Sun, H. X. Zang, S. Chen, S. D. Zhang, and K. W. Cheung, "Chance-constrained coordinated optimization for urban electricity and heat networks," *CSEE Journal of Power and Energy Systems*, vol. 4, no. 4, pp. 399–407, Dec. 2018.

[12] J. D. Wei, Y. Zhang, J. X. Wang, X. Y. Cao, and M. A. Khan, "Multi-period planning of multi-energy microgrid with multi-type uncertainties using chance constrained information gap decision method," *Applied Energy*, vol. 260, pp. 114188, Feb. 2020.

[13] M. Vrakopoulou, B. W. Li, and J. L. Mathieu, "Chance constrained reserve scheduling using uncertain controllable loads part I: Formulation and scenario-based analysis," *IEEE Transactions on Smart Grid*, vol. 10, no. 2, pp. 1608–1617, Mar. 2019.

[14] Z. C. Shi, H. Liang, S. J. Huang, and V. Dinavahi, "Distributionally robust chance-constrained energy management for islanded microgrids," *IEEE Transactions on Smart Grid*, vol. 10, no. 2, pp. 2234–2244, Mar. 2019.

[15] G. Chen, H. C. Zhang, H. X. Hui, and Y. H. Song, "Fast wasserstein-distance-based distributionally robust chance-constrained power dispatch for multi-zone HVAC systems," *IEEE Transactions on Smart Grid*, vol. 12, no. 5, pp. 4016–4028, Sep. 2021.

[16] W. J. Xie and S. Ahmed, "Distributionally robust chance constrained optimal power flow with renewables: A conic reformulation," *IEEE Transactions on Power Systems*, vol. 33, no. 2, pp. 1860–1867, Mar. 2018.

[17] A. Peña-Ordieres, D. K. Molzahn, L. A. Roald, and A. Wächter, "DC optimal power flow with joint chance constraints," *IEEE Transactions on Power Systems*, vol. 36, no. 1, pp. 147–158, Jan. 2021.

[18] G. Chen, H. C. Zhang, H. X. Hui, and Y. H. Song, "Deep-quantile-regression-based surrogate model for joint chance-constrained optimal power flow with renewable generation," *IEEE Transactions on Sustainable Energy*, vol. 14, no. 1, pp. 657–672, Jan. 2023.

[19] L. Yu, Y. P. Li, G. H. Huang, Y. R. Fan, and S. Nie, "A copula-based flexible-stochastic programming method for planning regional energy system under multiple uncertainties: A case study of the urban agglomeration of Beijing and Tianjin," *Applied Energy*, vol. 210, pp. 60–74, Jan. 2018.

[20] J. M. Grosso, C. Ocampo-Martínez, V. Puig, and B. Joseph, "Chance-constrained model predictive control for drinking water networks," *Journal of Process Control*, vol. 24, no. 5, pp. 504–516, May 2014.

[21] K. Baker and B. Toomey, "Efficient relaxations for joint chance constrained AC optimal power flow," *Electric Power Systems Research*, vol. 148, pp. 230–236, Jul. 2017.

[22] K. Baker and A. Bernstein, "Joint chance constraints in AC optimal power flow: Improving bounds through learning," *IEEE Transactions on Smart Grid*, vol. 10, no. 6, pp. 6376–6385, Nov. 2019.

[23] L. Roald and G. Andersson, "Chance-constrained AC optimal power flow: Reformulations and efficient algorithms," *IEEE Transactions on Power Systems*, vol. 33, no. 3, pp. 2906–2918, May 2018.

[24] A. Venzke, L. Halilbasic, U. Markovic, G. Hug, and S. Chatzivasileiadis, "Convex relaxations of chance constrained AC optimal power flow," *IEEE Transactions on Power Systems*, vol. 33, no. 3, pp. 2829–2841, May 2018.

[25] A. Venzke and S. Chatzivasileiadis, "Convex relaxations of probabilistic AC optimal power flow for interconnected AC and HVDC grids," *IEEE Transactions on Power Systems*, vol. 34, no. 4, pp. 2706–2718, Jul. 2019.

[26] Y. P. Zhang, X. M. Ai, J. Y. Wen, J. K. Fang, and H. B. He, "Data-adaptive robust optimization method for the economic dispatch of active distribution networks," *IEEE Transactions on Smart Grid*, vol. 10, no. 4, pp. 3791–3800, Jul. 2019.

[27] A. Velloso, A. Street, D. Pozo, J. M. Arroyo, and N. G. Cobos, "Two-stage robust unit commitment for Co-optimized electricity markets: An adaptive data-driven approach for scenario-based uncertainty sets," *IEEE Transactions on Sustainable Energy*, vol. 11, no. 2, pp. 958–969, Apr. 2020.

[28] X. Y. Cao, J. X. Wang, and B. Zeng, "Networked microgrids planning through chance constrained stochastic conic programming," *IEEE Transactions on Smart Grid*, vol. 10, no. 6, pp. 6619–6628, Nov. 2019.

[29] Y. Zhang, J. X. Wang, B. Zeng, and Z. C. Hu, "Chance-constrained two-stage unit commitment under uncertain load and wind power output using bilinear benders decomposition," *IEEE Transactions on Power Systems*, vol. 32, no. 5, pp. 3637–3647, Sep. 2017.

[30] Z. Y. Wang, B. K. Chen, J. H. Wang, M. M. Begovic, and C. Chen, "Coordinated energy management of networked microgrids in distribution systems," *IEEE Transactions on Smart Grid*, vol. 6, no. 1, pp. 45–53, Jan. 2015.

[31] S. X. Wang, S. J. Chen, L. J. Ge, and L. Wu, "Distributed generation hosting capacity evaluation for distribution systems considering the robust optimal operation of OLTC and SVC," *IEEE Transactions on Sustainable Energy*, vol. 7, no. 3, pp. 1111–1123, Jul. 2016.

[32] C. Shang, X. L. Huang, and F. Q. You, "Data-driven robust optimization based on kernel learning," *Computers & Chemical Engineering*, vol. 106, pp. 464–479, Nov. 2017.
[33] A. Patle and D. S. Chouhan, "SVM kernel functions for classification," in *Proceedings of 2013 International Conference on Advances in Technology and Engineering (ICATE)*, 2013, pp. 1–9.
[34] IEEE. Resources-IEEE PES test feeder. [Online]. Available: https://cmte.ieee.org/pes-testfeeders/resources/.
[35] Samples. [Online]. https://github.com/lelouchsola/SVCBasedOPF.
[36] F. Pedregosa, G. Varoquaux, A. Gramfort, V. Michel, B. Thirion, O. Grisel, M. Blondel, P. Prettenhofer, R. Weiss, V. Dubourg, J. Vanderplas, A. Passos, D. Cournapeau, M. Brucher, M. Perrot, and É. Duchesnay, "Scikit-learn: Machine learning in Python," *The Journal of Machine Learning Research*, vol. 12, pp. 2825–2830, Feb. 2011.
[37] C. S. Saunders, "Point estimate method addressing correlated wind power for probabilistic optimal power flow," *IEEE Transactions on Power Systems*, vol. 29, no. 3, pp. 1045–1054, May 2014.
[38] P. Li, X. H. Guan, J. Wu, and X. X. Zhou, "Modeling dynamic spatial correlations of geographically distributed wind farms and constructing ellipsoidal uncertainty sets for optimization-based generation scheduling," *IEEE Transactions on Sustainable Energy*, vol. 6, no. 4, pp. 1594–1605, Oct. 2015.

Ge Chen is an Assistant Professor in the School of Engineering at Great Bay University, Dongguan, China. He received the B.S. degree from Huazhong University of Science and Technology, Wuhan, China, in 2015, and the M.S. degree from Xi'an Jiaotong University, Xi'an, China, in 2018, both in Thermodynamic Engineering. He earned his Ph.D. degree in Electrical and Computer Engineering from the University of Macau, Macao, China, in 2023. From 2023 to 2025, he was a Postdoctoral Research Associate at Purdue University. His research interests include power system optimization and deep learning applications for intelligent decision-making.

Hongcai Zhang received the B.S. and Ph.D. degrees in Electrical Engineering from Tsinghua University, Beijing, China, in 2013 and 2018, respectively. From 2018 to 2019, he was a Post-Doctoral Scholar with the Energy, Controls, and Applications Laboratory, University of California at Berkeley, Berkeley, CA, USA, where he also worked as a Visiting Student Researcher in 2016. He is currently an Associate Professor with the State Key Laboratory of Internet of Things for Smart City and the Department of Electrical and Computer Engineering, University of Macau, Macao, China. He is also an Affiliated Researcher at the University of Macau Advanced Research Institute in Hengqin, Hengqin, China. His current research interests include urban energy systems, transportation electrification, and distributed energy resources.

Hongxun Hui received the B.E. and Ph.D. degrees in Electrical Engineering from Zhejiang University, Hangzhou, China, in 2015 and 2020, respectively. From 2018 to 2019, he was a Visiting Scholar with the Advanced Research Institute, Virginia Tech, Blacksburg, VA, USA, and also with the CURENT Center, University of Tennessee, Knoxville, TN, USA. He is currently an Assistant Professor with the State Key Laboratory of Internet of Things for Smart City, University of Macau, Macau, China. His research focuses on smart grid optimization and control, demand response, power economics, carbon markets, and interdisciplinary energy-environment systems.

Yonghua Song received the B.E. degree in Electrical Engineering from the Chengdu University of Science and Technology, Chengdu, China, in 1984, and the Ph.D. degree in Electrical Engineering from China Electric Power Research Institute, Beijing, China, in 1989. From 1989 to 1991, he was a Postdoctoral Fellow with Tsinghua University, Beijing. He held various positions with Bristol University, Bristol, U.K., Bath University, Bath, U.K., and John Moores University, Liverpool, U.K., from 1991 to 1996. In 1997, he was a Professor of power systems with Brunel University, Uxbridge, U.K., where he has been a Pro-Vice Chancellor for Graduate Studies since 2004. In 2007, he was a Pro-Vice Chancellorship and Professorship of electrical engineering with the University of Liverpool, Liverpool, U.K. In 2009, he joined Tsinghua University, Beijing, as a Professor of electrical engineering, an Assistant President, and the Deputy Director with the Laboratory of Low-Carbon Energy. From 2012 to 2017, he was the Executive Vice President with Zhejiang University, Hangzhou, China, the Founding Dean of the International Campus, and a Professor of electrical engineering and Higher Education. Since 2018, he has been a Rector with the University of Macau, Macao, China. His current research interests include smart grid, electricity economics, operation and control of power systems. Dr. Song was a recipient of the D.Sc. Award by Brunel University, in 2002, for his original achievements in power system research. In 2004, he was elected as a Fellow of the Royal Academy of Engineering, U.K.